Research Square

Preprints are preliminary reports that have not undergone peer review.
They should not be considered conclusive, used to inform clinical practice,
or referenced by the media as validated information.

Nonylphenol Promotes Colorectal Cancer Progression via the ERK–FosB Signaling Pathway

Weiwei Ning
Affiliated Hospital of Zunyi Medical University
Qingxu Yang
Affiliated Hospital of Zunyi Medical University
Zhengbiao Li
Affiliated Hospital of Zunyi Medical University
Ming Xie
xieming_xim@163.com

Affiliated Hospital of Zunyi Medical University

Research Article

Keywords: Nonylphenol, colorectal cancer, ERK1/2 MAP kinase, FosB, gene regulation

Posted Date: April 14th, 2026

DOI: https://doi.org/10.21203/rs.3.rs-9273972/v1

License: This work is licensed under a Creative Commons Attribution 4.0 International License. Read Full License

Additional Declarations: No competing interests reported.

Abstract

Purpose

Nonylphenol (NP) is a pervasive environmental endocrine disruptor, yet its mechanistic role in colorectal cancer (CRC) progression remains poorly defined. This study aimed to elucidate the molecular pathways through which NP influences CRC pathogenesis.

Methods

Human CRC cell lines HCT-116 and HT29 were treated with environmentally relevant NP concentrations. Functional assays assessed proliferation, apoptosis, cell cycle, migration, and invasion. RNA sequencing identified transcriptional changes, followed by validation via qPCR and western blot. Stable FosB knockdown and pharmacological MEK/ERK inhibition were employed to interrogate pathway necessity. A BALB/c nude mouse xenograft model was used for in vivo validation.

Results

Low-dose NP (100 nM) significantly enhanced proliferation, S-phase entry, migration, and invasion in CRC cells. Transcriptomic analysis revealed activation of the MAPK signaling pathway and marked upregulation of the AP-1 transcription factor FOSB. NP induced rapid ERK1/2 phosphorylation and FosB expression. Genetic knockdown of FOSB or pharmacological inhibition of MEK/ERK completely abolished NP-driven malignant phenotypes in vitro. In xenograft models, NP significantly accelerated tumor growth; this effect was abrogated by FOSB silencing, which also reversed NP-induced proliferation and suppressed apoptosis in vivo.

Conclusion

NP promotes CRC progression via the ERK1/2–FosB signaling axis. This pathway represents a critical mechanistic link between environmental NP exposure and aggressive CRC phenotypes, identifying FosB as a potential therapeutic target.

Introduction

Colorectal cancer (CRC) represents one of the most common malignant tumors of the digestive tract, posing a significant burden on global public health systems. It currently ranks third in global incidence (9.6%) and second in mortality (9.3%) among all malignant tumors(Bray et al., 2024; Keum and Giovannucci, 2019). According to the latest

GLOBOCAN estimates in 2022, the global burden continues to rise, with approximately 1.1 million new cases reported and about 900,000 deaths attributed to the disease(Bray et al., 2024). In China, colorectal cancer now ranks second among the causes of cancer-related deaths, with approximately 517,100 new cases and 240,000 deaths reported in 2022, reflecting rapid epidemiological transitions linked to urbanization, dietary shifts, and environmental changes(Han et al., 2024). In line with socio-economic development and changes in lifestyle, both incidence and mortality rates for CRC have shown a noticeable upward trend over the past decades(Foster, 2013; Zhu et al., 2017). Furthermore, CRC exhibits distinct demographic patterns, alongside a concerning global trend toward a younger age at diagnosis(Foster, 2013; Zhu et al., 2017). While advancements in early screening, surgical resection techniques, and systemic therapies have improved outcomes for patients with early-stage disease, the prognosis for metastatic CRC remains dismal, with a 5-year survival rate hovering at only 10–15%(Biller and Schrag, 2021; Van Cutsem et al., 2016). Hence, elucidating the molecular mechanisms underlying the occurrence, progression, and metastasis of CRC.

Environmental estrogens, also known as xenoestrogens, are a class of chemical substances present in the environment that possess estrogen-like activity. Causal relationships between environmental estrogens and metabolic disorders such as obesity, as well as hormone-sensitive cancers have been well established(Adeel et al., 2017). Nonylphenol (NP), a prototypical alkylphenol, is a degradation product of nonylphenol ethoxylates (NPEs), which are extensively used in products ranging from detergents to pesticides(Soares et al., 2008). Consequently, human exposure is widespread and chronic, evidenced by its detection in human urine, blood, breast milk, and adipose tissue(Calafat et al., 2005; Fernandez et al., 2007).

A growing body of evidence associates NP exposure with a spectrum of adverse health outcomes, including metabolic disruption, and immunotoxicity(Chen et al., 2015; Kharrazian, 2014). Studies show that NP can stimulate the proliferation of breast cancer cells (e.g., MCF-7) via estrogen receptor (ER)-α dependent and independent pathways(In et al., 2015), influence cell growth and apoptosis in prostate cancer models(Kim et al., 2016), and potentially contribute to uterine fibroid growth(Shen et al., 2014). A prior study indicated that NP could regulate cell growth in CRC cells(Yang et al., 2017), but the detailed signaling mechanism remains largely unexplored.

The biological effects of estrogenic compounds like NP are mediated through complex signaling networks. These are often initiated at the plasma membrane by receptors such as the G-protein coupled estrogen receptor 1 (GPER1, formerly GPR30)(Prossnitz and Arterburn, 2015; Prossnitz et al., 2007). Activation of these membrane-associated receptors can trigger cascades of kinase activities, prominently including the phosphoinositide 3-kinase (PI3K)/Akt and the mitogen-activated protein kinase (MAPK)

pathways(Levin, 2009). The MAPK/ERK1/2 module is a cardinal signaling hub that transmits extracellular to intracellular responses governing cell fate decisions(Dhillon et al., 2007). Constitutive or aberrant activation of the ERK1/2 pathway is a common feature in CRC(Fang and Richardson, 2005).

AP-1, typically composed of Jun (c-Jun, JunB, JunD) and Fos family proteins, binds to specific DNA sequences to regulate cell cycle progression, apoptosis, invasion, and angiogenesis(Eferl and Wagner, 2003). FosB have been implicated in cellular plasticity, stress responses, and oncogenesis. In various cancer contexts, FosB overexpression correlates with aggressive phenotypes and poor patient outcomes(Milde-Langosch, 2005; Tulchinsky, 2000). In CRC, elevated AP-1 activity is associated with advanced tumor stage and metastasis(Vaiopoulos et al., 2010).

In this study, we employed a multi-faceted approach combining *in vitro* functional assays in two distinct CRC cell lines (HCT-116 and HT29), transcriptomic analysis, targeted genetic intervention (FosB knockdown), pharmacological pathway inhibition, and *in vivo* validation using a murine xenograft model. Our comprehensive results provide compelling evidence for a defined signaling cascade linking environmental NP exposure to CRC progression through ERK1/2-FosB axis.

Materials and Methods

Cell Culture and Maintenance

Human colorectal carcinoma cell lines HCT-116 and HT29 were procured from Shanghai FuHeng Biotechnology were cultured in McCoy's 5A medium (Shanghai FuHeng Biotechnology, FH-A01) supplemented with 10% heat-inactivated FBS (Gibco, 10099-141) and 1% penicillin-streptomycin (Beyotime, C0222). HT29 cells (with mutant BRAF and PIK3CA) were maintained in DMEM (Shanghai BasalMedia Technology, L110KJ) supplemented with 10% FBS and 1% penicillin-streptomycin. Both cell lines were incubated at 37°C in a humidified atmosphere of 95% air and 5% CO□.

NP Treatment and Experimental Grouping

Nonylphenol was purchased from sigma (84852-15-3). A 100 mM stock solution was prepared in high-grade dimethyl sulfoxide (DMSO, Sigma-Aldrich, D2650) and stored at -20°C. Cells were treated with NP at final concentrations of 10 nM, 100 nM, and 1 μM for 24, 48, and 72 hours.

Cell Viability and Proliferation Assay

Cell proliferation was assessed using the Cell Counting Kit-8 (CCK-8) (Beyotime, C0038) assay. Cells were seeded in 96-well flat-bottom plates at a density of 5 × 10□ cells per well in 100 µL of complete medium. After overnight attachment (24 hours), cells were treated according to the experimental design. At the designated time points (24, 48, 72 hours), 10 µL of CCK-8 reagent was added directly to each well, and plates were incubated for an additional 2 hours at 37°C. The absorbance at 450 nm (reference wavelength 650 nm) was measured using a K6600-A microplate reader (Beijing Kaiao Technology).

Cell Apoptosis

Apoptosis was evaluated by flow cytometry using an Annexin V-PE/7-AAD-PerCP Apoptosis Detection Kit (MutiSciences Biotech, AP104-30). After the indicated treatments, both adherent and floating cells were harvested; adherent cells were detached using trypsin without EDTA and immediately combined with the corresponding culture supernatant to avoid loss of non-adherent or apoptotic cells. Cells were washed twice with ice-cold phosphate-buffered saline (PBS), and 10□ cells were resuspended in 500 µL of 1× binding buffer. Subsequently, 5 µL Annexin V-PE and 10 µL 7-AAD-PerCP were added, and the samples were gently mixed and incubated for 5 min at room temperature in the dark. Stained cells were analyzed immediately on a NovoCyte flow cytometer (ACEA Biosciences, USA) equipped with 488-nm and 561-nm lasers, with APC and 7-AAD fluorescence detected using 660/20-nm and 695/40-nm band-pass filters, respectively.

Cell Cycle Distribution Analysis

To analyze cell cycle progression, cells were seeded in 6-well plates (5 × 10□ cells/well). After 48 hours of culture, both adherent and floating cells were collected, combined, and washed twice with cold phosphate-buffered saline (PBS). Cells were fixed in ice-cold 70% ethanol and stored at -20°C for at least 4 hours. Prior to analysis, fixed cells were washed with PBS, treated with RNase A (MCE, HY-129046D) (100 µg/mL), and stained with propidium iodide (PI, 50 µg/mL) for 30 minutes at 37°C in the dark. Cellular DNA content was analyzed using a flow cytometer (NovoCyte, ACEA Biosciences) equipped with a 488 nm laser.

Transwell Invasion Assay

Invasion assays were performed using BioCoat™ Matrigel® Invasion Chambers (Corning). Prior to the assay, the Matrigel matrix (Beyotime, MC0383) (diluted to 200–300 µg/mL with serum-free medium) was applied to the upper surface of the membrane and allowed to polymerize at 37°C for 2 hours. Cells were harvested after treatment, washed, and resuspended in serum-free medium at a density of 2.5 × 10□ cells/mL. The upper chamber

was loaded with 100 µL of cell suspension (2.5 × 10⁵ cells). The lower chamber was filled with 600 µL of complete medium containing 20% FBS as a chemoattractant. After incubation for 48 hours at 37°C, non-invading cells on the upper surface of the membrane were gently removed with a cotton-tipped swab. Invaded cells on the lower surface were fixed with 70% methanol for 15 minutes, stained with 0.1% crystal violet for 20 minutes, and washed with distilled water. Membranes were air-dried and photographed under an inverted light microscope (XD, Ningbo Sunny Optical) at 200x magnification.

Wound Healing Migration Assay

Cells were seeded in 6-well plates and grown to near-confluent monolayers (~ 95%). A uniform scratch wound was created across the center of each well using a sterile 200 µL pipette tip. Detached cells were removed by washing three times with PBS. Fresh medium containing 2% FBS was added. Images of the wound were captured immediately (0 hour) and at specified intervals (24, 48, 72 hours) using an inverted microscope with a digital camera. The wound area at each time point was measured using the freehand selection tool in ImageJ software.

RNA Sequencing and Bioinformatics

Total RNA was extracted from HCT-116 cells treated with 100 nM NP or DMSO vehicle for 48 hours using RNAiso Plus (TaKaRa, 9109). RNA integrity was assessed using an Agilent Bioanalyzer (RIN > 8.0). Library construction and 150 bp paired-end sequencing on an Illumina NovaSeq 6000 platform were performed by a commercial service provider (Beijing Genomics Institute). Raw sequencing reads were processed to remove adapters and low-quality bases using Trimmomatic. Clean reads were aligned to the human reference genome (GRCh38) using HISAT2. Gene expression levels were quantified as fragments per kilobase of transcript per million mapped reads (FPKM) using StringTie. Differential expression analysis was conducted with DESeq2, applying a threshold of $|\log2(\text{fold change})| > 0.585$ (corresponding to a 1.5-fold change) and an adjusted p-value (Benjamini-Hochberg) < 0.05. Gene Ontology (GO) enrichment and Kyoto Encyclopedia of Genes and Genomes (KEGG) pathway analyses were performed using the clusterProfiler R package to identify significantly enriched biological processes and signaling pathways.

Quantitative Real-Time PCR (qPCR)

Total RNA from cultured cells or snap-frozen tumor tissues was extracted using RNAiso Plus (Takara, 9109). cDNA was synthesized from 1 µg of total RNA using the PrimeScript RT reagent Kit with gDNA Eraser (Takara, RR047A) in a 20 µL reaction. Quantitative PCR was performed on a qTOWER 3G Real-Time PCR System (Analytik Jena AG) using

PerfectStart Green qPCR SuperMix (TransGen, AQ601-02). The reaction conditions were: 94°C for 30 sec, followed by 40 cycles of 94°C for 5 sec and 60°C for 30 sec. Melt curve analysis was performed to confirm amplification specificity. The primer sequences used are listed below:

FosB-F: 5'-CATTGTCAACCTCGCCGC-3'

FosB-R: 5'-TGCTCGGTGCTGTCTGGAA-3'

CCNB1-F: 5'-GCAGCACCTGGCTAAGAATGT-3'

CCNB1-R: 5'-CAGCCTTGGCTAAATCTTGAACT-3'

CDC20-F: 5'-GCAGACATTCACCCAGCATCA-3'

CDC20-R: 5'-ATCCACGGCACTCAGACAGG-3'

GAPDH-F: 5'-CCAGAACATCATCCCTGCCT-3'

GAPDH-R: 5'-CCTGCTTCACCACCTTCTTG-3'

Relative gene expression was calculated using the comparative 2^(-ΔΔCt) method, with GAPDH serving as the endogenous reference gene for normalization.

Western Blot Analysis

Cells or homogenized tumor tissues were lysed in RIPA buffer (Beyotime, P0013B) supplemented with 1 mM PMSF and a protease/phosphatase inhibitor cocktail (Roche, 4693116001). Lysates were centrifuged at 14,000 × g for 15 minutes at 4°C. Protein concentration in the supernatant was determined using a BCA Protein Assay Kit (Pierce, 23225). Equal amounts of protein (10–20 µg) were separated by SDS-PAGE on 4–20% gradient mini-protean TGX gels (Bio-Rad) and transferred to PVDF membranes (Millipore). Membranes were blocked with 5% (w/v) bovine serum albumin (BSA) in TBST for 1 hour at room temperature and then incubated with primary antibodies diluted in blocking buffer overnight at 4°C. After three washes with TBST, membranes were incubated with appropriate HRP-conjugated secondary antibodies for 1 hour at room temperature. Protein bands were visualized using an enhanced chemiluminescence (ECL) substrate (ThermoFisher, 34579) and captured with a MiniChemi 610 imaging system (Beijing Saizhi). Primary antibodies used were: anti-FosB (HuaBio, ET1611-75), anti-ERK1/2 (Proteintech, 11257-1-AP), anti-phospho-ERK1/2 (Thr202/Tyr204) (Proteintech, 28733-1-AP), anti-CCNB1 (Proteintech, 28603-1-AP), anti-CDC20 (Proteintech, 10252-1-AP), anti-Ki-67 (Proteintech, 27309-1-AP), and anti-GAPDH (Proteintech, 10494-1-AP). HRP-conjugated secondary antibodies were from Jackson ImmunoResearch.

Lentiviral Vector Construction and FosB Knockdown

Three distinct shRNA oligonucleotide sequences targeting human FOSB (NM_006732) were designed and synthesized. The sequences were:

shFosB-1: 5'-CTCGCCTCTGTGAACTCTTT-3'

shFosB-2: 5'-CTTCGTACACTTCTTCGTTT-3'

shFosB-3: 5'-TCTTTACACACAGTGAGATT-3'

A non-targeting scrambled shRNA sequence (5'-TTCTCCGAACGTGTCACGT-3') served as the negative control (NC). Oligos were cloned into the pLKO.1-puro lentiviral vector (Addgene) between the BamHI and EcoRI restriction sites. Lentiviral particles were produced by co-transfecting 293T cells with the transfer vector and packaging plasmids (psPAX2 and pMD2.G) using polyethylenimine (PEI). Viral supernatants were collected at 48 and 72 hours post-transfection, filtered, and concentrated by ultracentrifugation. HCT-116 and HT29 cells were transduced with lentiviruses at an appropriate multiplicity of infection (MOI) in the presence of 8 μg/mL polybrene. Stable cell lines were selected with 2 μg/mL puromycin for 7–10 days.

In Vivo Xenograft Tumor Study

Thirty female BALB/c nude mice (4–6 weeks old, 19–23 g) were purchased from GemPharmatech (Chengdu) Co., Ltd. Mice were housed under specific pathogen-free (SPF) conditions. After one week of acclimatization, mice were randomly divided into six groups (n = 5 per group).

For tumor inoculation, exponentially growing cells were harvested, washed, and resuspended at 5*10 cells in 100 μL of serum-free medium, mixed 1:1 with cold Matrigel. The cell suspension (200 μL total) was injected subcutaneously into the right dorsal flank of each mouse using a 1 mL insulin syringe. Tumor growth was monitored every three days by measuring the length (L, longest dimension) and width (W, shortest perpendicular dimension) with digital calipers. Tumor volume was calculated using the formula: V = (L*W^2) / 2. Starting one week post-inoculation (when palpable tumors formed), mice in the NP treatment groups received intraperitoneal injections of NP (80 μM in 100 μL of saline containing 5% DMSO) every three days. Control groups received vehicle injections. On day 24, all mice were euthanized by cervical dislocation under deep anesthesia induced by intraperitoneal injection of Ketamine (50 mg/kg). Tumors were carefully excised, photographed, weighed, and measured. Each tumor was divided: one portion was fixed in

4% paraformaldehyde for 24 hours for histology, and the remainder was snap-frozen in liquid nitrogen for molecular analysis.

Histopathology, Immunohistochemistry (IHC), and TUNEL Assay

Formalin-fixed, paraffin-embedded tumor tissues were sectioned at 5 μm thickness. For general histopathology, sections were stained with hematoxylin and eosin (H&E) using a standard protocol(Magaki et al., 2019).

For Ki-67 IHC, antigen retrieval was performed by heating sections in citrate buffer (pH 6.0) in a microwave. Endogenous peroxidase activity was quenched with 3% H□O□. Sections were blocked with 10% normal goat serum and incubated overnight at 4°C with anti-Ki-67 antibody (Proteintech, 27309-1-AP) (1:200). After washing, sections were incubated with a biotinylated secondary antibody and then with HRP-conjugated streptavidin. Staining was developed with 3,3'-diaminobenzidine (DAB) substrate and counterstained with hematoxylin. For quantification, five representative high-power fields (HPF, 400x) per tumor section were captured. Apoptosis was detected using a One-Step TUNEL Apoptosis Assay Kit (Beyotime, C1089).

Statistical Analysis

Data are presented as the mean ± standard deviation (SD) from at least three independent experiments unless otherwise stated. Statistical analysis was performed using GraphPad Prism software (version 10.5.21). Normality of data distribution was assessed using the Shapiro-Wilk test. For comparisons between two groups, an unpaired two-tailed Student's t-test was used for data with normal distribution and equal variance; the Mann-Whitney U test was used for non-parametric data. For comparisons among multiple groups, one-way analysis of variance (ANOVA) was performed, followed by Tukey's post-hoc test for data meeting homogeneity of variance (assessed by Brown-Forsythe test) or by the Kruskal-Wallis test with Dunn's post-hoc test for non-parametric data. Differences in tumor growth curves over time were analyzed by two-way repeated measures ANOVA. A p-value of less than 0.05 was considered statistically significant. All statistical tests were two-sided. ns stands for no significance;*$P < 0.05$; **$P < 0.01$; ***$P < 0.001$; ****$P < 0.0001$.

Results

Low-Dose Nonylphenol Enhances the Proliferative Capacity of CRC Cells

To define the concentration range and temporal dynamics of NP's effects on CRC cells, we conducted a comprehensive CCK-8 viability screen. HCT-116 and HT29 cells were exposed

to a spectrum of NP concentrations (10 nM, 100 nM, 1 μM) for 24, 48, and 72 hours (Fig. 1A). 1 μM NP exerted a consistent inhibitory effect on cell viability, educing viability to 80–94% of control. In contrast, lower concentrations elicited a subtle but statistically significant pro-proliferative effect, particularly evident after 48 hours of exposure. Treatment with 100 nM NP for 48 hours increased the viability of HCT-116 cells to 106.02% ± 4.11% and HT29 cells to 105.10% ± 7.92% relative to their respective DMSO controls. These data indicate that NP, at environmentally plausible low doses, can function as a mitogenic stimulus for CRC cells, whereas higher doses are cytotoxic. Based on this profile, the condition of 100 nM NP for 48 hours was selected for all subsequent *in vitro* experiments.

NP Treatment Alters Cell Cycle Dynamics, Promoting S-Phase Entry

To elucidate the cellular basis for the observed increase in proliferation, we analyzed the cell cycle distribution. In HCT-116 cells, treatment with 100 nM NP for 48 hours resulted in a significant redistribution of cells among the cycle phases (Fig. 1B). Specifically, the percentage of cells in the G0/G1 phase decreased from 65.2% in controls to 61.3%, while the proportion of cells in the S phase increased markedly from 33.5% to 41.1%. The G2/M population remained relatively stable. This shift indicates that NP stimulates HCT-116 cells to transition from the G1 resting phase into the DNA synthesis (S) phase, thereby accelerating cell cycle progression. In HT29 cells, a similar trend was observed. These results confirm that the pro-proliferative effect of NP is associated with active modulation of the cell cycle machinery.

NP Potentiates the Migratory and Invasive Phenotypes of CRC Cells

In the wound healing assay (Fig. 1C), NP exposure accelerated the rate of wound closure. For instance, in HT29 cells, the wound healing percentage at 48 hours post-scratch was 41.9% in the NP-treated group versus 35.2% in the control group. As shown in Fig. 1D, NP treatment significantly augmented the invasive capacity of both HCT-116 and HT29 cells. The number of cells invading through the Matrigel-coated membrane increased by approximately 1.8-fold in HCT-116 and 1.6-fold in HT29 cells compared to their respective controls. These findings demonstrate that NP robustly enhances the migratory and invasive properties of CRC cells, key hallmarks of metastatic potential.

Transcriptomic Analysis Implicates MAPK Signaling and Identifies FosB as a Key Responder

To gain an unbiased, genome-wide perspective on the molecular changes induced by NP, we performed RNA sequencing on HCT-116 cells treated with 100 nM NP or vehicle for 48 hours. Differential expression analysis identified 1,247 genes that were significantly upregulated and 893 genes that were downregulated in response to NP (adjusted $p < 0.05$, $|\log2FC| > 0.5$). KEGG pathway enrichment analysis of the upregulated genes revealed highly significant enrichment for terms including "MAPK signaling pathway", "Transcriptional misregulation in cancer," "Cell cycle," and "Focal adhesion" (Fig. 2A). Within the list of most significantly upregulated genes, *FOSB*(encoding the FosB protein) emerged as a top candidate, with a log2 fold change of 1.92 (approximately 3.8-fold increase) (Fig. 2B).

NP Activates the ERK1/2 MAPK Pathway and Induces FosB Expression

Guided by the transcriptomic results, we examined the activation status of the ERK1/2 pathway, a major branch of MAPK signaling. Western blot analysis showed that NP treatment (100 nM, 48 hours) led to a pronounced increase in the levels of phosphorylated ERK1/2 (p-ERK1/2 at Thr202/Tyr204) in both HCT-116 and HT29 cells, while total ERK1/2 protein remained unchanged (Fig. 2C). Concurrently, NP exposure resulted in a substantial upregulation of FosB protein, consistent with the RNA-seq data (Fig. 2C). Quantitative PCR confirmed that NP induced a significant increase in *FOSB*mRNA levels (Fig. 2D).

Genetic Knockdown of FosB Abrogates NP-Induced Malignant Phenotypes

To establish the relationship between FosB upregulation and the biological effects of NP, we stably knocked down FosB expression in both cell lines using lentiviral shRNA. Three independent shRNA sequences were tested, and shFosB-2 was selected for all subsequent experiments, reducing FosB mRNA and protein levels by over 70% (Fig. 3A-B). Strikingly, FosB knockdown completely reversed the pro-proliferative effect of NP. In CCK-8 assays, while NP treatment boosted the viability of control (NC) cells (Fig. 3C). In cells transduced with control shRNA (shNC), treatment with 100 nM NP for 48 hours did not significantly alter the overall apoptotic rate. In contrast, when FOSB was stably knocked down (shFosB), subsequent NP exposure resulted in a pronounced increase in apoptosis (Fig. 3D). In transwell invasion assays, the NP-induced increase in invaded cell numbers was almost entirely abolished in shFosB cells (Fig. 3E). Similarly, wound healing assays demonstrated that the accelerated migration caused by NP was significantly blunted upon FosB silencing (Fig. 4A). These functional rescue experiments provide definitive evidence that FosB is an essential mediator required for NP to exert its tumor-promoting effects on CRC cell proliferation, migration, and invasion.

The ERK1/2 Pathway Acts Upstream of FosB and is Necessary for NP's Effects

We next investigated the hierarchical relationship between ERK1/2 activation and FosB induction. Western blot analysis showed that NP-induced ERK1/2 phosphorylation was partially attenuated in FosB-knockdown cells (Fig. 4B). To directly test the requirement of ERK1/2 signaling for NP's actions, we used the pharmacological MEK1/2 inhibitor PD98059. Pre-treatment with PD98059 effectively blocked NP-induced ERK1/2 phosphorylation (Fig. 4C). Crucially, this inhibition of the ERK1/2 pathway completely nullified the pro-proliferative effect of NP in the CCK-8 assay (Fig. 4C). This experiment positions ERK1/2 activation as an upstream, obligatory event for NP to stimulate cell proliferation, presumably through the subsequent induction of FosB and other targets.

NP Promotes Tumor Growth In Vivo in a FosB-Dependent Manner

To validate the pathophysiological relevance of our *in vitro* findings, we established subcutaneous xenograft models. NP administration significantly accelerated tumor growth of (Fig. 5A). For HT29-derived tumors, the final average tumor volume in the NP + NC group (1023.98 ± 94.54 mm³) was substantially larger than in the NC group (696.53 ± 100.87 mm³) at day 24. A similar effect was observed with HCT-116 tumors: NP + NC volume = 1088.16 ± 152.32 mm³ vs. NC volume = 647.53 ± 241.83 mm³. The most compelling result was that the tumor-promoting effect of NP was almost completely abrogated in mice injected with FosB-knockdown cells (NP+shFosB groups). The tumor volumes in these groups (e.g., 691.31 ± 107.64 mm³ for HCT116/NP+shFosB) were not significantly different from those in the untreated NC groups and were dramatically smaller than in the NP + NC groups (Fig. 5B).

FosB Mediates NP-Induced Proliferation and Suppression of Apoptosis in Tumors

Gross examination and H&E staining, revealed that NP + NC tumors were generally larger, more fleshy, and exhibited higher cellularity with fewer necrotic (Fig. 5C). In contrast, NP+shFosB tumors often showed more extensive regions of necrosis. Immunohistochemical staining for Ki-67 demonstrated that NP treatment significantly increased the proliferative index, while this increase was markedly suppressed in FosB-knockdown tumors treated with NP (Fig. 5D). Conversely, the TUNEL assay for apoptosis detection showed that NP exposure reduced the apoptotic index in NC tumors, suggesting enhanced survival. This anti-apoptotic effect of NP was reversed in the NP+shFosB group, where the apoptotic index returned to levels similar to the NC group (Fig. 6A). These *in*

vivo histopathological findings confirm that FosB is crucial for mediating NP's dual effects of stimulating proliferation and inhibiting apoptosis within the tumor microenvironment.

Molecular Profiling of Tumors Confirms Activation of the ERK1/2–FosB Axis

The mRNA levels of key proliferation and cell cycle-related genes, *CCNB1* (Cyclin B1) and *CDC20* (Cell Division Cycle 20), were significantly elevated in NP + NC tumors but were significantly lower in NP+shFosB tumors (Fig. 6B). NP treatment increased the p-ERK1/2/ERK1/2 ratio and FosB protein abundance in control tumors. Importantly, these increases were attenuated in tumors derived from FosB-knockdown cells (Fig. 6C). The protein levels of CCNB1 and CDC20 followed a similar pattern, being induced by NP in a FosB-dependent manner.

Discussion

The biphasic dose-response observed in our viability assays—proliferation at low doses (10–100 nM) and inhibition at a higher dose (1 μM)—is a hallmark characteristic of many EDCs and hormones(Vandenberg et al., 2012). The selected active concentration of 100 nM is plausible within the context of chronic, low-level human exposure. The concomitant shift in cell cycle distribution towards the S phase provides a clear cellular mechanism for the increased proliferation, aligning with the known role of estrogenic signals in promoting G1/S transition through induction of cyclins and suppression of CDK inhibitors(Prall et al., 1997).

Our transcriptomic approach was pivotal in identifying FosB as a key nodal point. While previous studies on NP in cancer have focused on classical estrogen receptors or the PI3K/Akt pathway(Amaro et al., 2014; In et al., 2015), our unbiased screen highlighted the MAPK/ERK1/2 pathway and its downstream transcriptional network. FosB's marked induction is particularly interesting. Unlike the transient expression of c-Fos, FosB and its truncated splice variant ΔFosB can exhibit remarkable stability, leading to sustained AP-1 activity that drives long-term adaptive and, in pathological contexts, maladaptive cellular responses(Nestler, 2015). In cancer, FosB/ΔFosB has been linked to therapy resistance, stem-like properties, and metastasis in breast and lung cancers(Milde-Langosch, 2005; Zhao et al., 2020). Our study is among the first to implicate FosB as a critical effector in environmental chemical-driven CRC progression.

The ERK1/2 inhibitor PD98059 blocked NP-induced proliferation, placing ERK1/2 activation upstream as the necessary trigger. The partial reduction of ERK1/2 phosphorylation in FosB-knockdown cells suggests a positive feedback loop. Such loops, where transcription factors sustain the activity of upstream kinases, are common in

cancer(Santos et al., 2007). This implies that once the NP-ERK1/2-FosB axis is engaged, it may become self-reinforcing, potentiating long-lasting effects even after NP exposure ceases.

Therapeutically, the ERK1/2–FosB axis presents a potential target for intervention. While directly targeting transcription factors like FosB remains challenging, inhibitors of the upstream kinase MEK (and thus ERK1/2) are already in clinical use or development for cancers with MAPK pathway mutations(Zhao and Adjei, 2014). Our data suggest that such inhibitors might be particularly relevant for CRC patients with a history of significant environmental EDC exposure or for preventing progression in high-risk settings.

Conclusion

In summary, this study delineates a novel and coherent signaling pathway through which the environmental contaminant nonylphenol promotes colorectal cancer progression. We demonstrate that NP, at environmentally relevant low doses, activates the ERK1/2 MAP kinase pathway, leading to the transcriptional induction of the AP-1 transcription factor FosB. FosB is functionally essential, acting as a critical downstream effector that mediates NP's stimulatory effects on cancer cell proliferation, migration, invasion *in vitro*, and tumor growth *in vivo*. The ERK1/2–FosB axis thus emerges as a key mechanistic link between exposure to this pervasive endocrine disruptor and the acquisition of aggressive cancer phenotypes.

Declarations

Acknowledgments

We extend our sincere gratitude to the technical staff at the Core Facility of Chongqing Life Knowledge Source Technology Co., Ltd. for their expert assistance with flow cytometry, animal experiments, and histology. We also thank our collaborators at Zunyi Medical University for their insightful discussions. This work was supported by the Health Commission of Guizhou Province (Grant No. gzwkj-2023-154) and the Basic Research Program of the Department of Science and Technology of Guizhou Province (Grant No. ZK [2023] General 557).

Author Contributions

Weiwei Ning and Ming Xie designed the project. Weiwei Ning performed most experiments. Qingxu Yang performed animal experiments. Zhengbiao Li performed the bioinformatic analysis. Weiwei Ning and Ming Xie wrote the manuscript.Conflicts of Interest.

Ethics approval and consent to participate

This study was reviewed and approved by the Ethics Committee of the Affiliated Hospital of Zunyi Medical University (Approval No. KLL-2022-431; date of approval: March 15, 2022). All animal procedures were conducted in accordance with the National Institutes of Health Guide for the Care and Use of Laboratory Animals and the guidelines of the Institutional Animal Care and Use Committee.

Competing interests

The authors declare that they have no competing interests.

Data Availability

The raw RNA sequencing data generated in this study will be deposited in the Gene Expression Omnibus (GEO) database upon acceptance. All other data supporting the findings of this study are available within the article and its supplementary information files or from the corresponding author upon reasonable request.

References

1. Adeel M, Song X, Wang Y, Francis D, Yang Y (2017) Environmental impact of estrogens on human, animal and plant life: A critical review. Environ Int 99:107–119
2. Amaro AA, Esposito AI, Mirisola V, Mehilli A, Rosano C, Noonan DM, Albini A, Pfeffer U, Angelini G (2014) Endocrine disruptor agent nonyl phenol exerts an estrogen-like transcriptional activity on estrogen receptor positive breast cancer cells. Curr Med Chem 21:630–640
3. Biller LH, Schrag D (2021) Diagnosis and Treatment of Metastatic Colorectal Cancer: A Review. JAMA 325:669–685
4. Bray F, Laversanne M, Sung H, Ferlay J, Siegel RL, Soerjomataram I, Jemal A (2024) Global cancer statistics 2022: GLOBOCAN estimates of incidence and mortality worldwide for 36 cancers in 185 countries. CA Cancer J Clin 74:229–263
5. Calafat AM, Kuklenyik Z, Reidy JA, Caudill SP, Ekong J, Needham LL (2005) Urinary concentrations of bisphenol A and 4-nonylphenol in a human reference population. Environ Health Perspect 113:391–395
6. Chen J, Xiao Y, Gai Z, Li R, Zhu Z, Bai C, Tanguay RL, Xu X, Huang C, Dong Q (2015) Reproductive toxicity of low level bisphenol A exposures in a two-generation zebrafish assay: Evidence of male-specific effects. Aquat Toxicol 169:204–214
7. Dhillon AS, Hagan S, Rath O, Kolch W (2007) MAP kinase signalling pathways in cancer. Oncogene 26:3279–3290

8. Eferl R, Wagner EF (2003) AP-1: a double-edged sword in tumorigenesis. Nat Rev Cancer 3:859–868
9. Fang JY, Richardson BC (2005) The MAPK signalling pathways and colorectal cancer. Lancet Oncol 6:322–327
10. Fernandez MF, Arrebola JP, Taoufiki J, Navalon A, Ballesteros O, Pulgar R, Vilchez JL, Olea N (2007) Bisphenol-A and chlorinated derivatives in adipose tissue of women. Reprod Toxicol 24:259–264
11. Foster PA (2013) Oestrogen and colorectal cancer: mechanisms and controversies. Int J Colorectal Dis 28:737–749
12. Han B, Zheng R, Zeng H, Wang S, Sun K, Chen R, Li L, Wei W, He J (2024) Cancer incidence and mortality in China, 2022. J Natl Cancer Cent 4:47–53
13. In SJ, Kim SH, Go RE, Hwang KA, Choi KC (2015) Benzophenone-1 and nonylphenol stimulated MCF-7 breast cancer growth by regulating cell cycle and metastasis-related genes via an estrogen receptor alpha-dependent pathway. J Toxicol Environ Health A 78:492–505
14. Keum N, Giovannucci E (2019) Global burden of colorectal cancer: emerging trends, risk factors and prevention strategies. Nat Rev Gastroenterol Hepatol 16:713–732
15. Kharrazian D (2014) The Potential Roles of Bisphenol A (BPA) Pathogenesis in Autoimmunity. Autoimmune Dis 2014, 743616
16. Kim SH, Nam KH, Hwang KA, Choi KC (2016) Influence of hexabromocyclododecane and 4-nonylphenol on the regulation of cell growth, apoptosis and migration in prostatic cancer cells. Toxicol Vitro 32:240–247
17. Levin ER (2009) Plasma membrane estrogen receptors. Trends Endocrinol Metab 20:477–482
18. Magaki S, Hojat SA, Wei B, So A, Yong WH (2019) An Introduction to the Performance of Immunohistochemistry. Methods Mol Biol 1897:289–298
19. Milde-Langosch K (2005) The Fos family of transcription factors and their role in tumourigenesis. Eur J Cancer 41:2449–2461
20. Nestler EJ (2015) ΔFosB: a transcriptional regulator of stress and antidepressant responses. Eur J Pharmacol 753:66–72
21. Prall OW, Sarcevic B, Musgrove EA, Watts CK, Sutherland RL (1997) Estrogen-induced activation of Cdk4 and Cdk2 during G1-S phase progression is accompanied by increased cyclin D1 expression and decreased cyclin-dependent kinase inhibitor association with cyclin E-Cdk2. J Biol Chem 272:10882–10894
22. Prossnitz ER, Arterburn JB (2015) International Union of Basic and Clinical Pharmacology. XCVII. G Protein-Coupled Estrogen Receptor and Its Pharmacologic Modulators. Pharmacol Rev 67:505–540

23. Prossnitz ER, Arterburn JB, Sklar LA (2007) GPR30: A G protein-coupled receptor for estrogen. Mol Cell Endocrinol 265–266:138–142
24. Santos SD, Verveer PJ, Bastiaens PI (2007) Growth factor-induced MAPK network topology shapes Erk response determining PC-12 cell fate. Nat Cell Biol 9:324–330
25. Shen Y, Ren ML, Feng X, Gao YX, Xu Q, Cai YL (2014) Does nonylphenol promote the growth of uterine fibroids? Eur J Obstet Gynecol Reprod Biol 178:134–137
26. Soares A, Guieysse B, Jefferson B, Cartmell E, Lester JN (2008) Nonylphenol in the environment: a critical review on occurrence, fate, toxicity and treatment in wastewaters. Environ Int 34:1033–1049
27. Tulchinsky E (2000) Fos family members: regulation, structure and role in oncogenic transformation. Histol Histopathol 15:921–928
28. Vaiopoulos AG, Papachroni KK, Papavassiliou AG (2010) Colon carcinogenesis: Learning from NF-kappaB and AP-1. Int J Biochem Cell Biol 42:1061–1065
29. Van Cutsem E, Cervantes A, Adam R, Sobrero A, Van Krieken JH, Aderka D, Aguilar A, Bardelli E, Benson A, Bodoky A, G. et al (2016) ESMO consensus guidelines for the management of patients with metastatic colorectal cancer. Ann Oncol 27:1386–1422
30. Vandenberg LN, Colborn T, Hayes TB, Heindel JJ, Jacobs DR Jr., Lee DH, Shioda T, Soto AM, vom Saal FS, Welshons WV et al (2012) Hormones and endocrine-disrupting chemicals: low-dose effects and nonmonotonic dose responses. Endocr Rev 33:378–455
31. Yang X, Huang H, Wang M, Zheng X, Xu J, Xie M (2017) Effect of nonylphenol on the regulation of cell growth in colorectal cancer cells. Mol Med Rep 16:2211–2216
32. Zhao Y, Adjei AA (2014) The clinical development of MEK inhibitors. Nat Rev Clin Oncol 11:385–400
33. Zhao Z, Sun W, Guo Z, Zhang J, Yu H, Liu B (2020) Mechanisms of lncRNA/microRNA interactions in angiogenesis. Life Sci 254:116900
34. Zhu J, Tan Z, Hollis-Hansen K, Zhang Y, Yu C, Li Y (2017) Epidemiological Trends in Colorectal Cancer in China: An Ecological Study. Dig Dis Sci 62:235–243

Figures

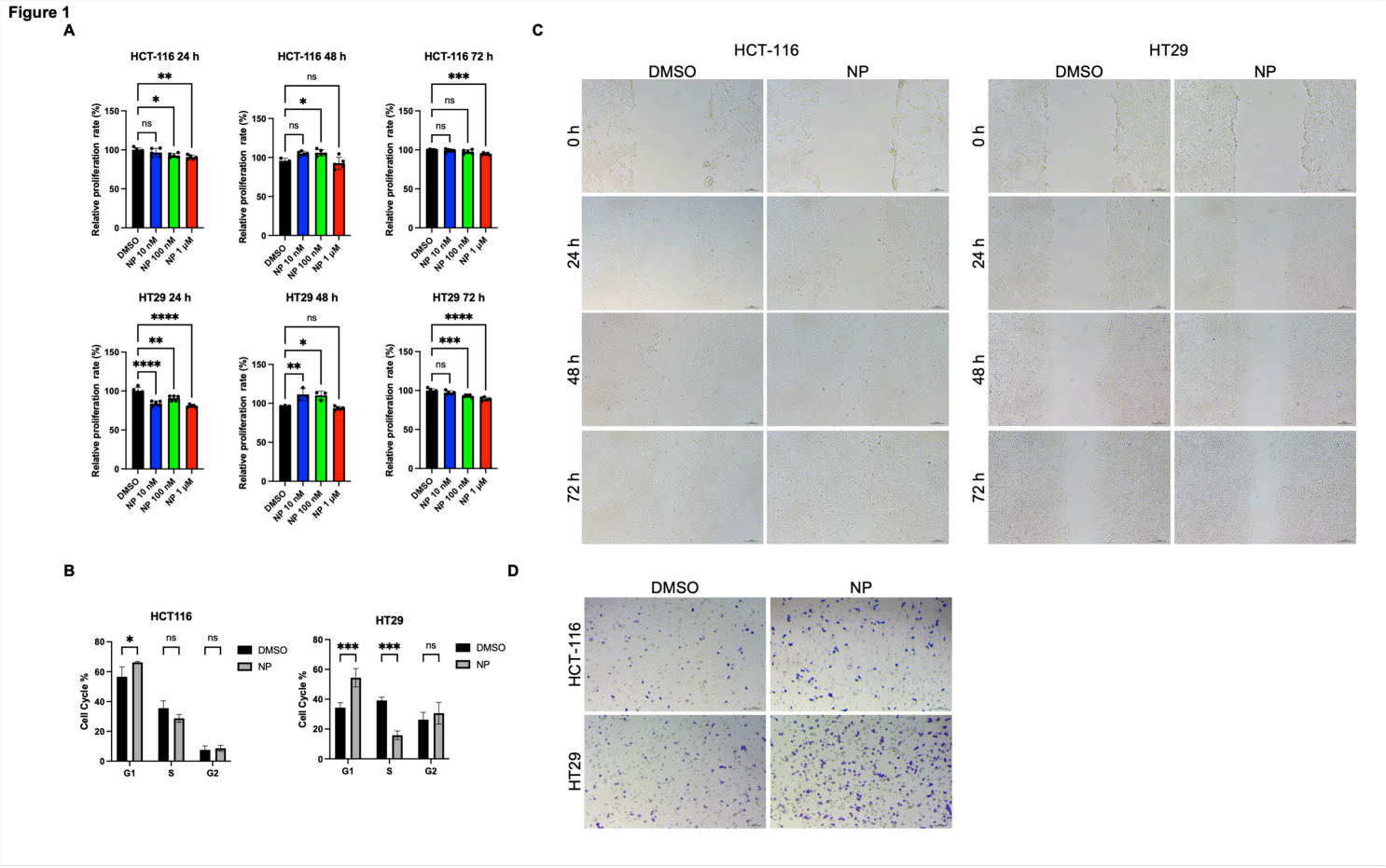


Figure 1

Nonylphenol promotes proliferation, cell cycle progression, migration, and invasion in CRC cells.

(A) HCT-116 and HT29 cells were treated with increasing concentrations of NP (10 nM, 100 nM, 1 μM) or vehicle control (DMSO) for 24, 48, and 72 hours. Cell viability was assessed by CCK-8 assay and was presented as a percentage relative to the DMSO control (set at 100%) at each time point. Data are shown as mean ± SD (n=5). (B) Cell cycle distribution was analyzed by flow cytometry after PI staining of HCT-116 and HT29 cells treated with 100 nM NP or DMSO for 48 hours. (C) Representative images of wound healing. Confluent monolayer of HCT116 and HT29 cells was scratched and then treated with 100 nM NP or DMSO. Wound closure was monitored and quantified at 0, 24, 48 and 72 hours. Scale bar = 100 μm. (D) Representative images of transwell invasion assays. HCT-116 and HT29 cells treated with 100 nM NP or DMSO for 48 hours were seeded into Matrigel-coated chambers. Invaded cells were stained with crystal violet and counted. Scale bar = 50 μm. Student’s t-test; ns stands for no significance;*P<0.05; **P<0.01; ***P<0.001; ****P<0.0001.

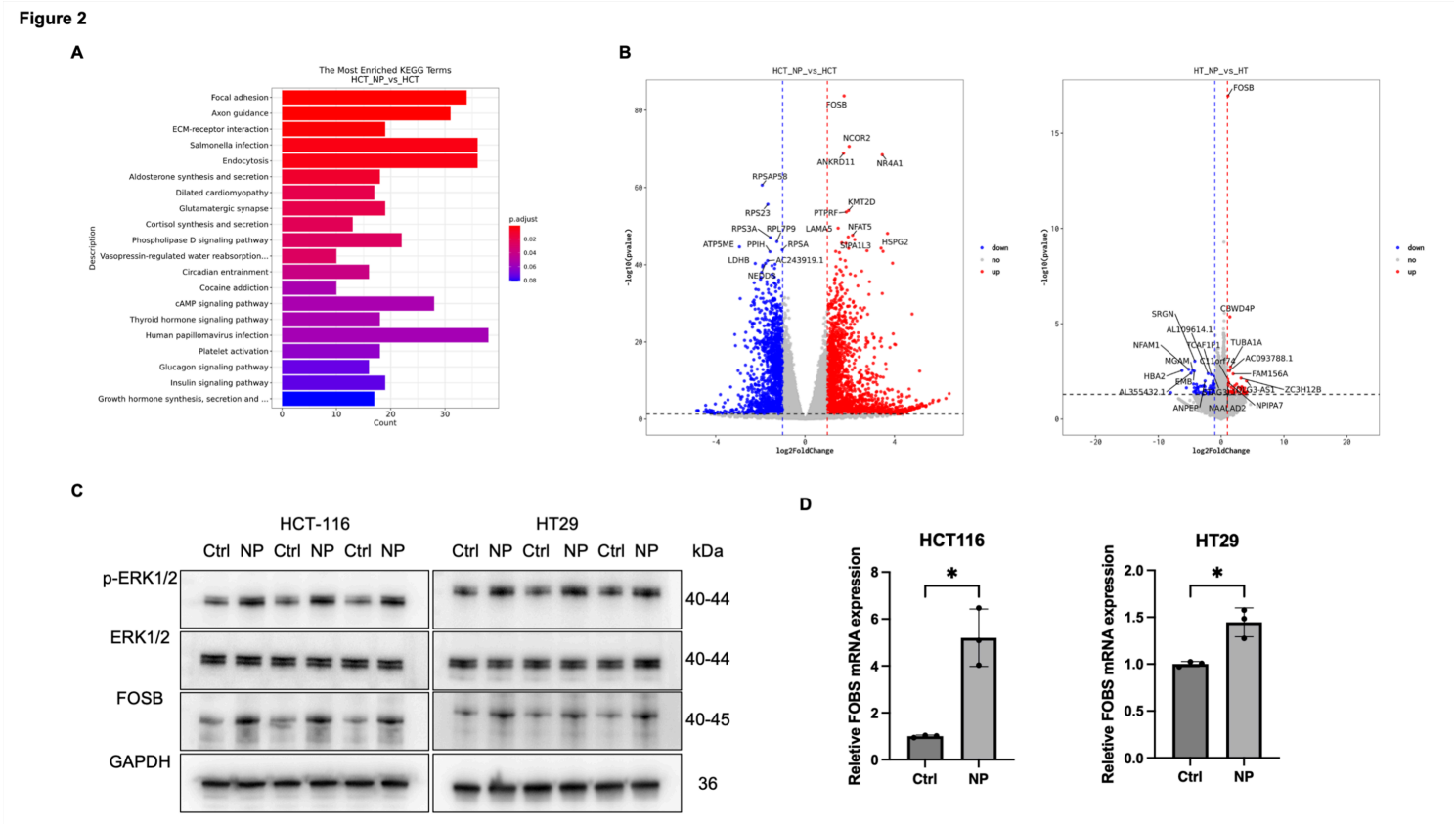


Figure 2

NP activates the MAPK pathway and upregulates FosB expression.

(A) HCT-116 cells were treated with 100 nM NP or DMSO for 48 hours, and transcriptomic changes were analyzed by RNA-seq. KEGG pathway enrichment analysis of significantly upregulated genes shows the top enriched pathways, including the MAPK signaling pathway. The size of the dot represents the gene count, and the color represents the adjusted p-value. (B) A volcano plot from the RNA-seq data highlights differentially expressed genes. The red and blue dots represent significantly upregulated and downregulated genes, respectively (|log2FC| > 0.5, padj < 0.05). (C) HCT-116 and HT29 cells were treated with 100 nM NP or DMSO for 48 hours. WB analysis ofphosphorylated ERK1/2 (p-ERK1/2), total ERK1/2 (t-ERK1/2), and FosB. GAPDH served as a loading control. (D) FOSB mRNA expression levels in HCT-116 and HT29 cells treated as in (C) were measured by qRT-PCR. Data are presented as mean ± SD from three independent experiments. Student’s t-test; *P<0.05.

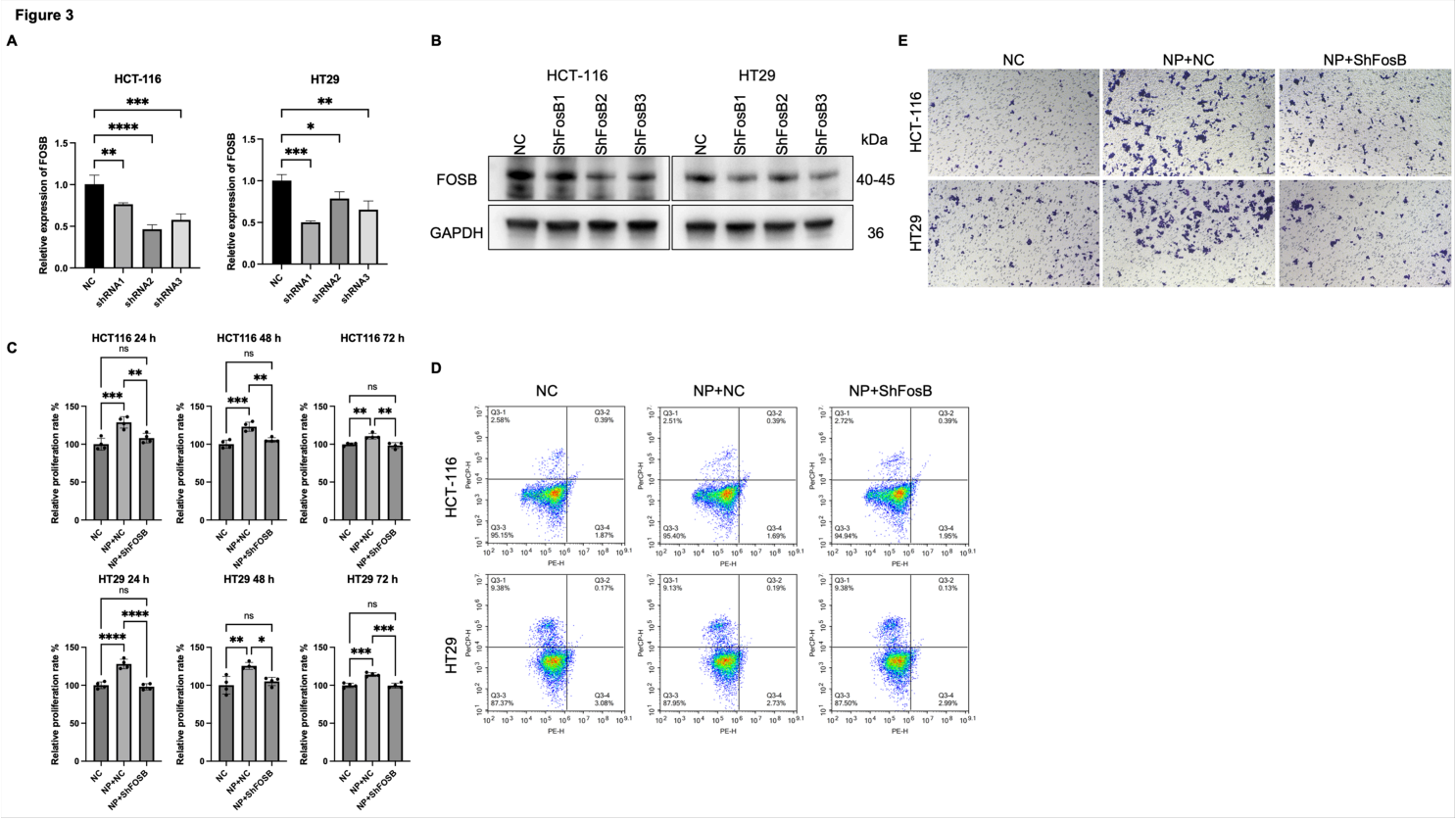


Figure 3

FosB knockdown abrogates NP-Induced proliferation, survival, and invasion.

(A-B) Validation of FosB knockdown efficiency in HCT-116 and HT29 cells stably transduced with control shRNA (NC) or FosB-targeting shRNA. (A) FOSB mRNA levels were measured by qRT-PCR. Data are shown as mean ± SD (n=3). (B) FosB protein levels were detected by Western blot. (C-E) Cells were treated with 100 nM NP or DMSO for 48 hours. (C) Cell viability was assessed by CCK-8 assay and was shown as a percentage of the untreated shNC control. Data are shown as mean ± SD (n=4). (D) Apoptosis was analyzed by flow cytometry after Annexin V-PE/7-AAD staining. Representative dot plots are shown. (E) Cell invasion was assessed using transwell assays. Representative images were shown. Scale bar = 100 μm. Student's t-test; ns stands for no significance;*P<0.05; **P<0.01; ***P<0.001; ****P<0.0001.

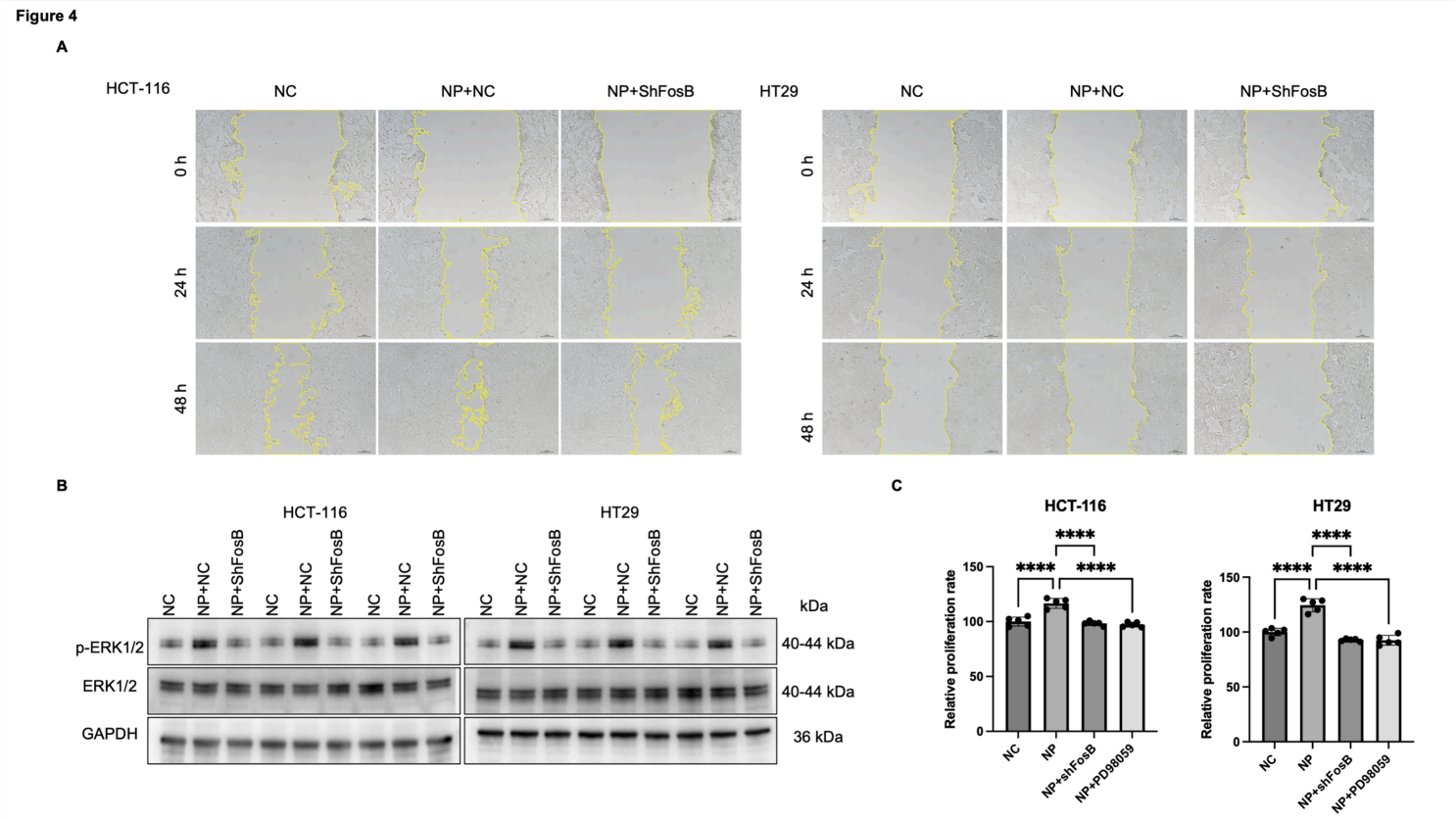


Figure 4

The ERK1/2 Pathway acts upstream of FosB to mediate NP's effects.

(A) Wound healing assays were performed in HCT-116 and HT29 cells. shNC and shFosB cells treated with 100 nM NP or DMSO. (B) shNC and shFosB cells were treated with 100 nM NP or DMSO for 48 hours. WB analysis of p-ERK1/2, ERK1/2 and FosB. (C) HCT-116 cells were pre-treated with the MEK inhibitor PD98059 (10 µM) or vehicle for 1 hour, followed by co-treatment with 100 nM NP or DMSO for 48 hours. Cell viability was assessed by CCK-8 assay and was shown as a percentage of the untreated control (right). Data are shown as mean ± SD (n=5). Student’s t-test; ns stands for no significance; ****P<0.0001.

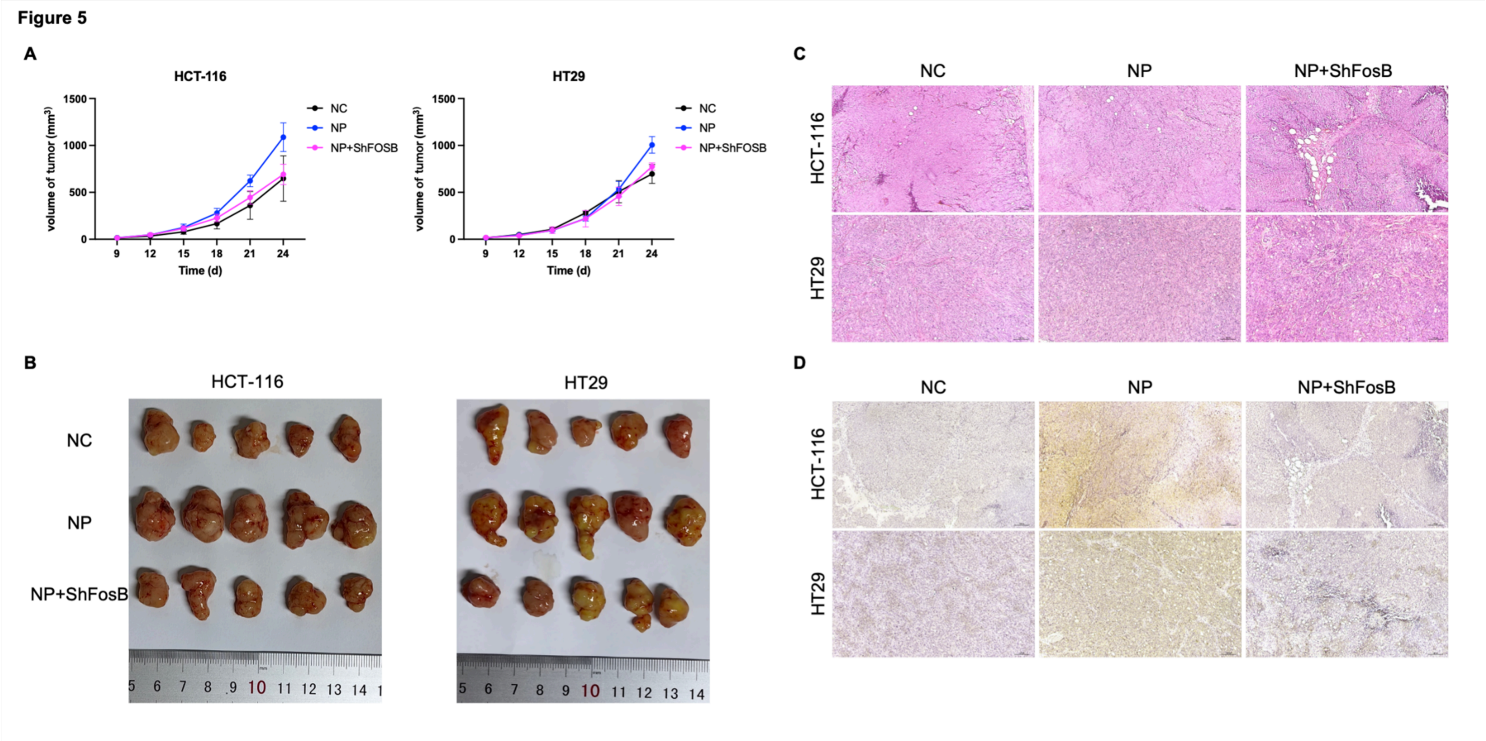


Figure 5

FosB is required for NP-promoted tumor growth in vivo.

BALB/c nude mice were subcutaneously injected with HCT-116 or HT29 cells stably expressing shNC or shFosB. Mice received intraperitoneal injections of NP (100 μM) or vehicle every three days.

(A) Tumor volumes were measured at the indicated time points (n=5 per group). Data are shown as mean tumor volume ± SD. (B) Images of excised tumors from each group at the end of the experiment (Day 24). (C) Representative images of H&E staining of tumor sections from the indicated groups. Scale bar = 100 μm. (D) Immunohistochemical staining for the proliferation marker Ki-67 in tumor sections. Representative images (left) and quantification of the Ki-67 positive index (right) are shown. Scale bar = 100 μm.

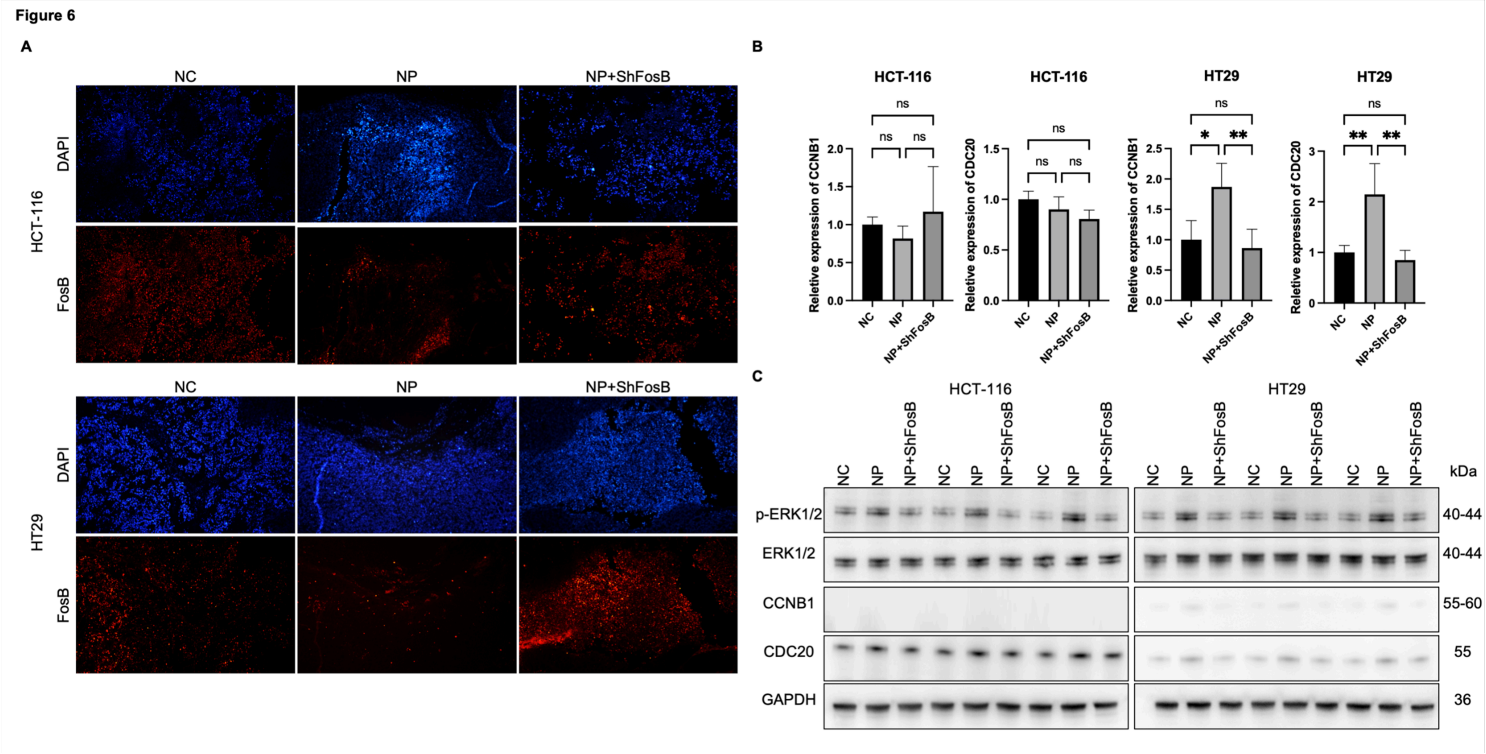


Figure 6

FosB mediates NP-induced proliferation and suppresses apoptosis in tumors.

(A) TUNEL assay was performed on tumor sections from the indicated groups. Nuclei were counterstained with DAPI (blue). Representative images are shown. Scale bar = 50 μm. (B) RNA was extracted from xenograft tumors. The mRNA expression levels of CCNB1 and CDC20 were measured by qRT-PCR and normalized to GAPDH. (C) Protein was extracted from xenograft tumors. The levels of p-ERK1/2, t-ERK1/2, FosB, CCNB1, and CDC20 were detected by Western blot. GAPDH served as a loading control. Data are shown as mean ± SD (n=4). Student’s t-test; ns stands for no significance;*P<0.05; **P<0.01.